

IGR J17252–3616: an accreting pulsar observed by *INTEGRAL* and *XMM-Newton*

J.A. Zurita Heras^{1,2}, G. De Cesare^{3,4,5}, R. Walter^{1,2}, A. Bodaghee^{1,2}, G. Bélanger⁸, T.J.-L. Courvoisier^{1,2}, S.E. Shaw^{6,1}, and J.B. Stephen⁷

¹ INTEGRAL Science Data Centre, ch. d'Ecogia 16, 1290 Versoix, Switzerland

² Observatoire de Genève, ch. des Maillettes 51, 1290 Sauverny, Switzerland

³ IASF-INAF, Via Fosso del Cavaliere 100, 00133 Roma, Italy

⁴ Dipartimento di Astronomia, Università degli Studi di Bologna, Via Ranzani 1, I40127 Bologna, Italy

⁵ Centre d'Etude Spatiale des Rayonnements, CNRS/UPS, B.P. 4346, 31028 Toulouse Cedex 4, France

⁶ School of Physics and Astronomy, University of Southampton, Highfield, SO17 1BJ, UK

⁷ IASF/CNR, Via Piero Gobetti 101, 40129 Bologna, Italy

⁸ Service d'Astrophysique, DAPNIA/DSM/CEA, 91191 Gif-sur-Yvette, France

Received / Accepted

Abstract. The discovery of the X-ray source IGR J17252–3616 by *INTEGRAL* was reported on 9 February 2004. Regular monitoring by *INTEGRAL* shows that IGR J17252–3616 is a persistent hard X-ray source with an average count rate of 0.96 counts s⁻¹ (~6.4 mCrab) in the 20–60 keV energy band. A follow-up observation with *XMM-Newton* which was performed on 21 March 2004, showed that the source is located at R.A. (2000.0) = 17^h25^m11.4^s and Dec. = –36°16′58.6″ with an uncertainty of 4″. The only infra-red counterpart to be found within the *XMM-Newton* error circle was 2MASS J17251139–3616575, which has a Ks-band magnitude of 10.7 and is located 1″ away from the *XMM-Newton* position.

The analysis of the combined *INTEGRAL* and *XMM-Newton* observations shows that the source is a binary X-ray pulsar with a spin period of 413.7 s and an orbital period of 9.72 days. The spectrum can be fitted with a flat power law plus an energy cut off ($\Gamma \sim 0.02$, $E_c \sim 8.2$ keV) or a Comptonized model ($kT_e \sim 5.5$ keV, $\tau \sim 7.8$). The spectrum also indicates a large hydrogen column density of $N_H \sim 15 \cdot 10^{22}$ atoms cm⁻² suggesting an intrinsic absorption. The Fe K α line at 6.4 keV is clearly detected. Phase-resolved spectroscopy does not show any variation in the continuum except the total emitted flux. The absorption is constant along the pulse phase. This source can be associated with EXO 1722–363 as both systems show common timing and spectral features. The observations suggest that the source is a wind-fed accreting pulsar accompanied by a supergiant star.

Key words. Gamma rays: observations, X-rays: binaries, pulsars: individual: IGR J17252–3616=EXO 1722–363

1. Introduction

X-ray binaries consist of a compact object, either a black hole or a neutron star, accreting matter from a companion star; they are usually classified according to the mass of the companion as a high mass (HMXB, $M_C \gtrsim 10 M_\odot$), intermediate-mass (IMXB, $M_C = 1\text{--}10 M_\odot$) or low mass X-ray binary (LMXB, $M_C \lesssim 1 M_\odot$). The LMXB and IMXB accrete matter through Roche-Lobe overflow from the companion star and through an accretion disk around the compact object (Tauris & van den Heuvel 2005).

The HMXB can be divided into two categories as the companion star can be either an OB supergiant or a Be star. OB supergiant stars feed the compact object through strong stellar winds and/or in some cases Roche-Lobe overflow. Be stars expell matter around their equator that fuels the compact ob-

ject. The orbits of Be binary systems are eccentric and generally have a longer period than OB supergiant systems ($\gtrsim 15$ days). The X-ray emission of HMXB presents a wide variety of patterns: from transient to persistent, outbursts on different times scales (seconds, days and/or years), periodic modulations, eclipses and others. Strongly magnetized neutron stars accompanied by massive stars show periodic pulsations; the accreted matter is funneled towards the poles by the magnetic field leading to an increase of the observed X-ray emission when these regions cross the line of sight. These HMXB usually show a hard X-ray spectrum between 2–10 keV with an energy cutoff around 10 keV.

Several new hard X-ray sources have been discovered by *INTEGRAL* (Winkler et al. 2003) in surveys of the galactic plane. Most of them have been detected by IBIS/ISGRI (Ubertini et al. 2003; Lebrun et al. 2003), the most sensitive instrument on board *INTEGRAL* between 20 and 300 keV. The brightest sources detected during the first year of the

INTEGRAL mission are listed in Bird *et al.* (2004). A few tens of them have never been detected before *INTEGRAL*'s observation. Most of these new objects show common features in their spectra, such as a high intrinsic low-energy absorption, and they are believed to be HMXB (Walter *et al.* 2003; Rodriguez *et al.* 2003; Patel *et al.* 2004).

IGR J17252–3616's discovery was reported on February 9, 2004, with 13 other hard X-ray sources (Walter *et al.* 2004) detected with ISGRI in all-sky mosaic images built from core programme data. However, there is evidence that IGR J17252–3616 has already been observed with previous missions. A galactic plane scan performed by *EXOSAT* in June 1984 revealed a point like X-ray source emission, GPS 1722–363 (Warwick *et al.* 1988), at a position not compatible with IGR J17252–3616 but with a low accuracy. *Ginga* observations in 1987 and 1988 confirmed the presence of a powerful X-ray accretor neutron star, X1722–36, with a pulsation of 413.9 s and important variations of the intensity in X-rays (Tawara *et al.* 1989). The source also showed a hard spectrum with important low-energy absorption and an emission line at 6.2 keV. Further investigations with *Ginga* in 1988 confirmed the spectral analysis, and lower limits for the orbital period of 9 days and the mass of the primary star of 15 M_{\odot} were deduced from pulse timing analysis (Takeuchi *et al.* 1990). Both investigations conclude that the system is a HMXB. Recently, those results were confirmed by Corbet *et al.* (2005) using *RXTE* data. They also found an orbital period of 9.741 ± 0.004 d.

IGR J17252–3616 is regularly monitored by *INTEGRAL*. A follow-up observation lasting three hours was performed with the X-ray Multi-Mirror Mission (*XMM-Newton*) on 21 March 2004. The new data available on this source is presented in this paper. *INTEGRAL* and *XMM-Newton* observations and data analysis techniques are described in Sects. 2 and 3, respectively. The results are presented in Sect. 4 and discussed in Sect. 5. The conclusions are presented in Sect. 6.

2. Observations

2.1. INTEGRAL

INTEGRAL is a hard X-ray and γ -ray observatory of the European Space Agency (ESA) launched on 17 October 2002. The payload consists of four instruments: the imager IBIS with two detector layers, ISGRI (20 keV–1 MeV) and PICsIT (200 keV–10 MeV, Labanti *et al.* (2003)); the spectrometer SPI (20 keV–8 MeV, Vedrenne *et al.* (2003)); the X-ray monitor JEM-X (3–30 keV, Lund *et al.* (2003)) and the optical camera OMC (V filter, Mas-Hesse *et al.* (2003)). Most of the *INTEGRAL* observing time is spent in the Galactic Plane.

IGR J17252–3616 is located close to the Galactic Centre, which has been observed regularly. The observing strategy consists of pointings each lasting ~ 30 minutes distributed in various grids around the Galactic Plane. The focus of the effort for this paper is on IBIS/ISGRI, since IBIS/PICsIT and SPI are less sensitive at energies lower than 300 keV where the source is detected. We did not use data from the JEM-X instrument because its smaller field of view and the dithering observation approach of *INTEGRAL* mean that the effective exposure

on IGR J17252–3616 is ten times smaller than obtained with ISGRI.

The data set consists of core programme data obtained until MJD 53341.1 and of public data obtained until MJD 52928.3, giving a total exposure of 6.5 Ms. Table 1 lists the source visibility periods, and for each of them the fraction of the time when the source was effectively observed in the partially-coded field of view (PCFOV).

2.2. XMM-Newton

IGR J17252–3616 was observed by *XMM-Newton* (Jansen *et al.* 2001) on 21 March 2004, from 13:02:45 to 16:04:45 UTC (MJD 53085.544–53085.671) for a total exposure of 11 ks. *XMM-Newton* operates with three instruments that cover the optical/UV and X-ray spectral bands. The main instrument for the purpose of this work is the European Photon Imaging Camera (EPIC) instrument, which consists of two MOS (Turner *et al.* 2001) and one pn (Strüder *et al.* 2001) CCD cameras. EPIC has a 30' field of view, and coverage of the 0.15–12 keV energy range with imaging, timing and spectral capabilities. The EPIC/MOS[12] and pn were all operating in imaging science mode with a large window and a medium filter.

The *XMM-Newton* observation was simultaneous with three *INTEGRAL* pointings in revolution 175 between MJD 53085.542 and 53085.667. However, the signal to noise (S/N) of ISGRI data during those simultaneous observations was too low to perform cross analysis.

3. Data Analysis

3.1. INTEGRAL

The data were reduced with the Offline Scientific Analysis version 4.2 software (OSA 4.2) that is publicly released by the *INTEGRAL* Science Data Centre (ISDC) (Courvoisier *et al.* 2003). All the pointings for which the source was either within the ISGRI fully coded (FCFOV, $9^{\circ} \times 9^{\circ}$) or partially coded (PCFOV, $29^{\circ} \times 29^{\circ}$) fields of view were analysed. Around 3000 pointings, distributed between revolutions 37 and 244, were selected. Sky images were extracted for each pointing and combined into mosaic images with longer exposures. As the source is weak, light curves were extracted from the imaging results (pointings and mosaics). During flares, light curves were extracted on shorter time scales using `ii_light` v7.3. Extracting high-energy spectra with OSA 4.2 remains a difficult task for faint sources. Spectra were extracted using `ii_spectra_extract` v2.3.1 and from the mosaic images, and compared. In the energy range in which the source is detected, both methods give consistent results. The redistribution matrix and ancillary response files (RMF and ARF) used were `isgr_rmfp_0012.fits` and `isgr_arf_rsp_0006.fits`, respectively. The RMF was rebinned in to 17 channels. Average fluxes and the source position were obtained from the mosaic images with `mosaic_spec` v1.0¹.

¹ `ii_light` and `ii_spectra_extract` are OSA 4.2 standard tools. `mosaic_spec` is released with OSA 5.0.

Table 1. The *INTEGRAL* Data set. We selected all public and core programme revolutions when IGR J17252–3616 was within the ISGRI PCFOV of $29^\circ \times 29^\circ$. The observing time fraction was calculated as the ratio between the net exposure time on the source and the elapsed time during the visibility periods.

Visibility Periods	Start [MJD]	End [MJD]	Revolutions	Observing time fraction
1	52671	52752	37–63	0.23
2	52859	52925	100–121	0.51
3	53050	53116	164–185	0.20
4	53236	53294	226–244	0.16

3.2. XMM-Newton

The Science Analysis System (SAS) version 6.1.0 was used to produce new event lists for the EPIC instrument running `epchain` for pn and `emchain` for MOS[12]. The event lists were corrected for enhanced background features at energies higher than 10 keV, disregarding time lapses when count rates above 10 keV exceeded 4 counts s^{-1} for pn, 1 count s^{-1} for MOS1 and 1 count s^{-1} for MOS2. Finally, only 5.9 ks of 9.2 ks, 6.2 ks of 10.7 ks and 7.0 ks of 10.7 ks for each instrument, respectively, were kept as good time intervals.

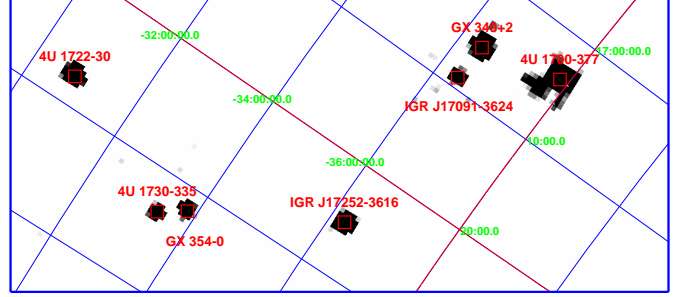
Images were built from the cleaned event lists for the MOS[12] and pn cameras with $2''$ and $4''$ resolution, respectively. Bad pixels were disregarded and good events were selected until the quadruple level. The lower threshold was fixed at 0.8 keV as recommended in the calibration status documentation (see calibration document XMM-SOC-CAL-TN-0018², p25).

To find the source location, the SAS task `edetect_chain` was used on each individual EPIC camera. Four images, with energy ranges of 0.5–2, 2–4.5, 4.5–7.5 and 7.5–12 keV, were created. The source position was calculated as the mean of the best position from each MOS and pn camera.

The source was clearly visible in the pn images in CCD 1, near the read-out node. An event list of source+background counts was selected from a circle of $50''$ around the bright object. The background was estimated from a region adjacent to the source region, with a similar size and at the same distance from the read-out node in the same CCD. To build light curves, only single and double events with an energy between 0.4 and 10 keV were collected, as advocated in the user guide. The background light curve was subtracted using the `FTOOLS` `lcmath`.

Source+background and background spectra were extracted from all EPIC cameras, MOS[12] and pn, disregarding bad pixels and selecting single and double events. Specific redistribution matrix and ancillary response files were generated for each EPIC instrument with the standard tasks `rmfgen` and `arfgen`, respectively. An average spectrum of the source from the complete observation was first obtained and the `Xspec` version 11.3.1 package was used to fit and plot the resulting spectra corrected for the background.

For the phase-resolved spectra, the `Xselect` version 2.2 software was used to select events corresponding to a specific



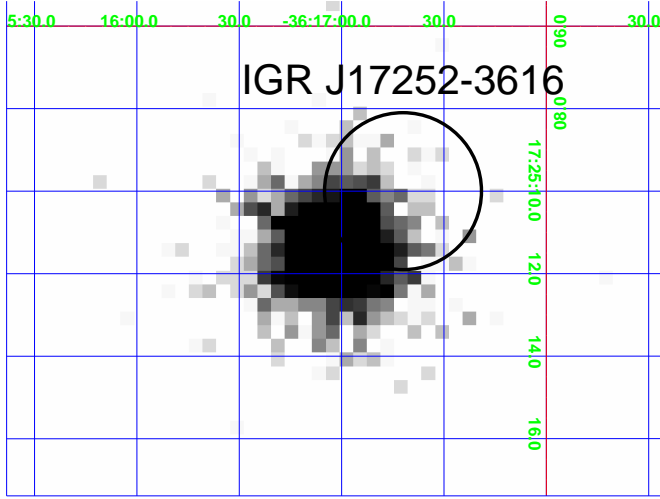


Fig. 2. IGR J17252–3616 EPIC/MOS1 image with the 23'' *INTEGRAL*/ISGRI error circle

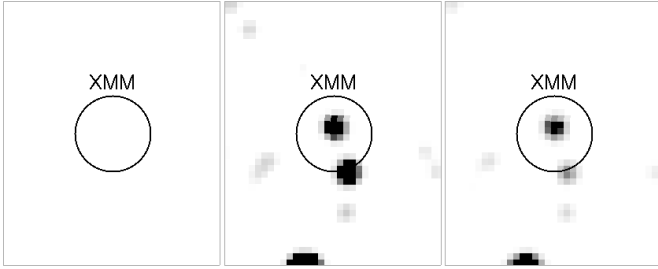


Fig. 3. Infrared counterpart of IGR J17252–3616. Images taken from the 2MASS survey: J-band (left), H-band (middle) and K-band (right). The EPIC error circle of 4'' is displayed. 2MASS J17251139-3616575 is only present in the H and K images.

Fig. 3). The colours obtained when dereddening those infrared magnitudes can either be interpreted as a close cool star or a distant hot star (Walter *et al.* 2005).

4.2. Timing analysis

4.2.1. Long-term variability

The long term variability of IGR J17252–3616 was studied using ISGRI data in two energy ranges: 20–60 keV and 60–150 keV. Mosaic images were built for each three days revolution and light curves extracted for both energy bands. When the source was not detected, 3σ flux upper limits were calculated. Net exposures higher than 5 ks at the source location were considered. Typical net exposures for one revolution vary from a few ks to several tens of ks. The source was never detected above 60 keV. The 3σ 60–150 keV average count rate upper limit is ~ 0.3 counts s^{-1} (~ 7 mCrab) with the highest and lowest values being ~ 0.6 counts s^{-1} (~ 14 mCrab) and ~ 0.6 counts s^{-1} (~ 3.5 mCrab). The 20–60 keV light curve on the time scale of a spacecraft revolution is shown in Fig. 4.

The source is detected in almost every single revolution. Its average 20–60 keV flux is 0.96 ± 0.01 counts s^{-1} (~ 6.4 mCrab), derived from a 20–60 keV mosaic image generated with data

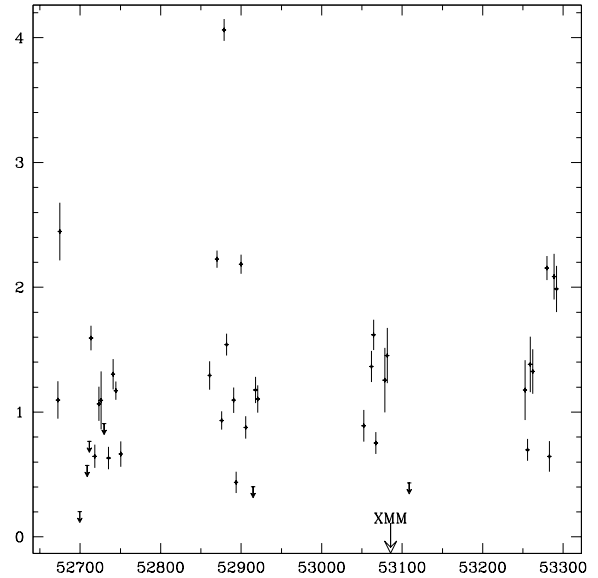


Fig. 4. IGR J17252–3616 20–60 keV light curve with average count rate per revolution (~ 3 days). 3σ upper limits are indicated when the source was not detected. The *XMM-Newton* observation time is shown.

of the first three visibility periods for a total net exposure of 1.7 Ms. The average flux of the object selecting only revolutions when the source is detected is 1.39 ± 0.02 counts s^{-1} (~ 9.3 mCrab) as calculated from Fig. 4. When selecting revolutions for which only upper limits are available (rev. 46, 49, 50, 56, 118 and 183) and building a mosaic image with a net exposure of 165 ks, the source is detected with a significance of 5σ , and the mean 20–60 keV flux reaches 0.19 ± 0.04 counts s^{-1} (~ 1.3 mCrab); this is five times less than the average mean flux over all the revolutions and seven times less than the average flux over revolutions when the source was detected. Nevertheless, the source is persistent as, once cumulating enough exposure time, it remains detectable.

On revolution time scales, the source flared up to 4 counts s^{-1} (~ 27 mCrab), or a factor of 10 stronger than the lowest detection of 0.4 counts s^{-1} (~ 2.7 mCrab), on one occasion (see Fig. 4). IGR J17252–3616 varies by a factor ~ 4 outside of this flare.

Variability on time scales shorter than a single revolution was also investigated. Light curves based on flux per pointing were built considering the full *INTEGRAL* data set in the 20–60 keV energy range. The source is often not detected in single pointings. The average count rate per pointing when the source is detected with a significance higher than 4σ varies between 2 and 4 counts s^{-1} (~ 13 – 27 mCrab) outside the flares. Four flares are detected in total, three in the 2nd visibility period and one in the 4th visibility period. The brightest flare occurred at MJD 52879 when the flux increased from ~ 2 counts s^{-1} to a peak of 10 counts s^{-1} (~ 67 mCrab) and decreased again in ~ 1 day (see Fig. 5). The other flares reached a flux level of ~ 6 – 8 counts s^{-1} (~ 40 – 53 mCrab) and lasted less than one day. Considering the

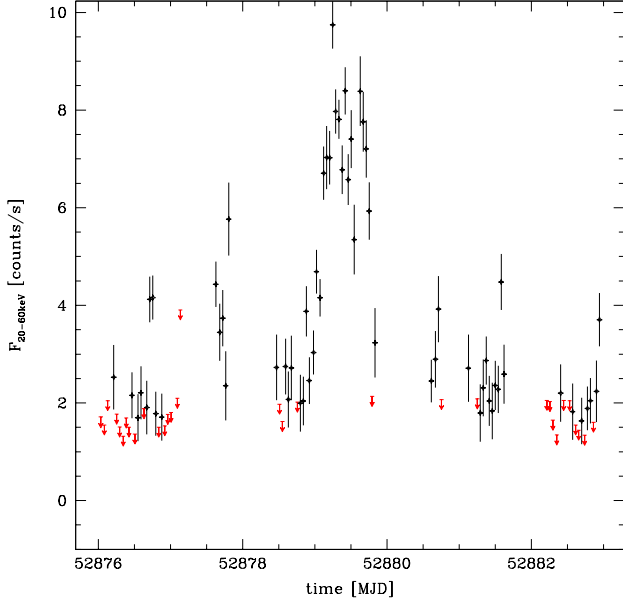


Fig. 5. IGR J17252–3616 20–60 keV light curve with average count rates per pointing (~ 30 min). Around MJD 52879, we observe the brightest flare during the four visibility periods. 3σ upper limits are indicated when the source was not detected.

observed count rates limit values of 0.2 and 10 counts s^{-1} , the source varies by a factor of more than 50 between different epochs.

4.2.2. Pulse period

Fig. 6 shows the *XMM-Newton* light curve. A periodic oscillation of ~ 400 s is clearly visible. A power spectral density distribution was created from the entire light curve in order to search for periodicity. A main peak was found around ~ 400 s with a harmonic at 200 s.

Starting from the estimated period, the best period was searched for in the χ^2 distribution when folding the light curve over a range of different periods. A significant peak was obtained, giving the best period of 414.8 ± 0.5 s when fitted with a Gaussian (see Fig. 7 top). The uncertainty on the period was estimated using Eq. 14 of Horne & Baliunas (1986) and Eq. 2 of Hill *et al.* (2005). Lomb-Scargle periodograms were generated using Press & Rybicki (1989) fast method. The light curve was folded with the best period to obtain the pulse profile between 0.4–10 keV (see Fig. 7 bottom). The *XMM-Newton* folded light curve is defined so that the minimum flux is set at phase 0 corresponding to MJD 53085.55144. A first local maximum is observed at phase ~ 0.15 followed by a broad maximum at phase ~ 0.6 . The pulse fraction, defined as $P_f = (I_{\max} - I_{\min}) / (I_{\max} + I_{\min})$ with I_{\max} and I_{\min} being the maximum and minimum intensities of the folded light curve, respectively, reaches $68 \pm 3\%$.

An ISGRI 50 s binned light curve was made during the bright flare observed at MJD 52879 in two energy bands 20–40 keV and 40–60 keV. Epoch folding the *INTEGRAL* data, start-

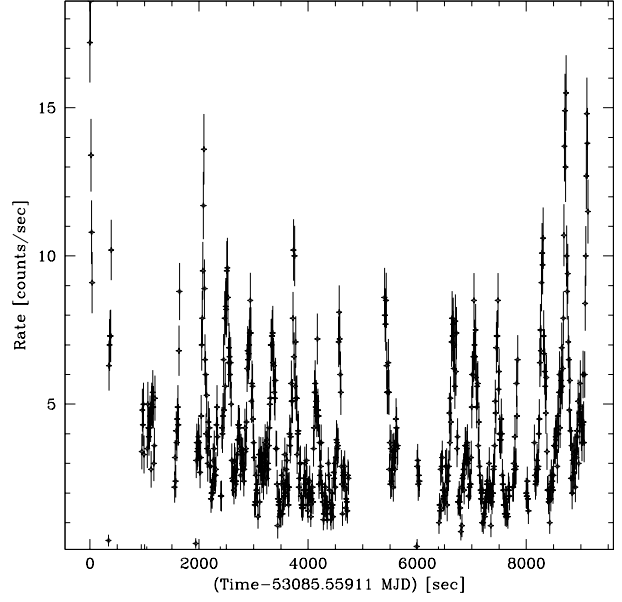


Fig. 6. IGR J17252–3616 EPIC/pn 10 s binned light curve. The gaps correspond to the periods with enhanced background activity that were discarded before starting the analysis.

ing with the period found in the EPIC/pn light curve, returned a period of 413.7 ± 0.3 s in the 20–40 keV band (see Fig. 8 top). The signal to noise of the 40–60 keV light curve is not significant enough to detect the modulation. The pulse profile shape shows a broad peak without complex structures (see Fig. 8 bottom). The pulse fraction reaches $56 \pm 12\%$ and is consistent with the value observed between 0.4–10 keV.

The shape of the X- and γ -ray pulse profiles show some differences. Due to the less significant detection in the ISGRI data, the number of phase bins is different in the pn and ISGRI folded light curves. The main peak in ISGRI seems broader than in pn. There is also a hint of a secondary peak in the pn data that is absent in the ISGRI data. The folded light curves cannot be compared in phase, because the phase 0 of both pulse profiles do not correspond in time as the observations are separated by 7 months. Notice that the 20–60 keV source intensity was three times brighter during the flare (MJD 52879) than during the *XMM-Newton* observation (\sim MJD 53085.6) (see Fig. 4).

4.2.3. Orbital period

Indications of an orbital period in the 20–60 keV light curve were searched for, based on flux per pointing. A Lomb-Scargle periodogram was generated between 4 and 28 days. The periods with flaring activity were removed in the light curve before searching for any coherent modulation. A significant peak at 9.72 ± 0.09 days is visible and the folded light curve is shown in Fig. 9. A minimum flux consistent with an eclipse is visible at phase 0. It lasts between phases 0.97–1.1 that corresponds to a lapse of time of ~ 1.26 days. The normalized intensity smoothly increases from phase 0.1 to 0.3 to reach a plateau that lasts ~ 3.9 days. Afterwards, the intensity gradually decreases from

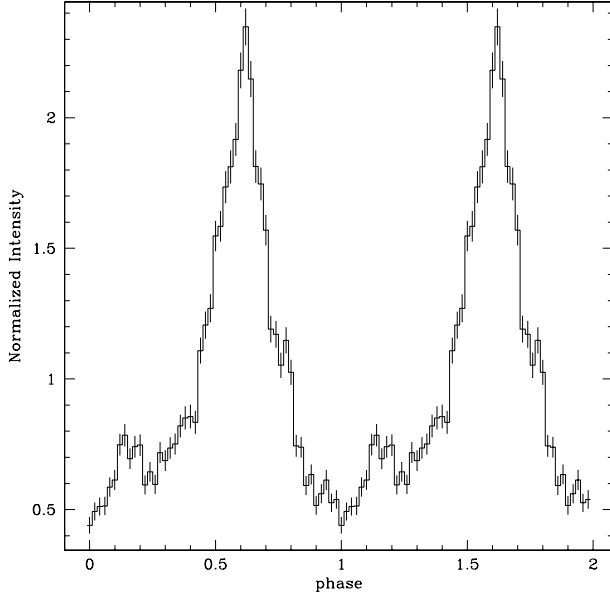
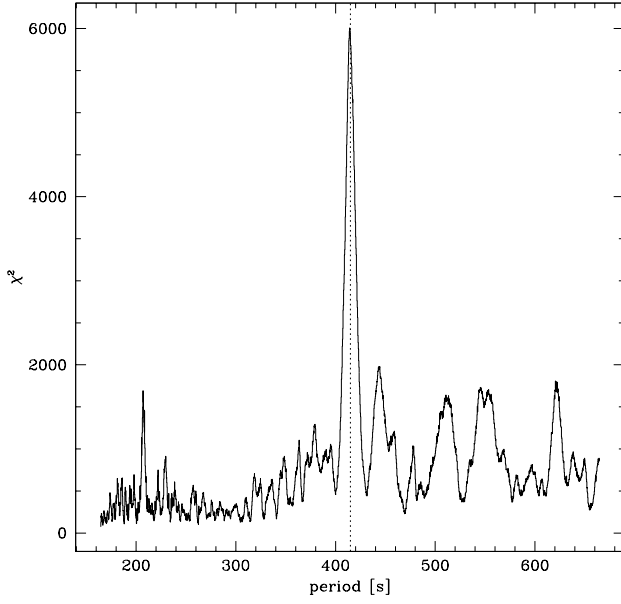


Fig. 7. *top:* χ^2 distribution of trials periods for epoch folding search on EPIC/pn data. The best value was fitted with a Gaussian. The best period of 414.8 ± 0.5 s is indicated with a dashed-line. *bottom:* IGR J17252–3616 pulse phase folded light curve in the 0.4–10 keV energy band obtained with the best spin period. The zero epoch is MJD 53085.55144.

phase 0.7 to the start of the eclipse at phase 0.97. The *XMM-Newton* observation corresponds to phase ~ 0.7 .

4.3. Spectral analysis

The X-ray spectral bins were grouped to have at least 100 counts per channel (see Fig. 10). This allows the use of the χ^2 statistic. The spectrum is strongly absorbed at energies lower

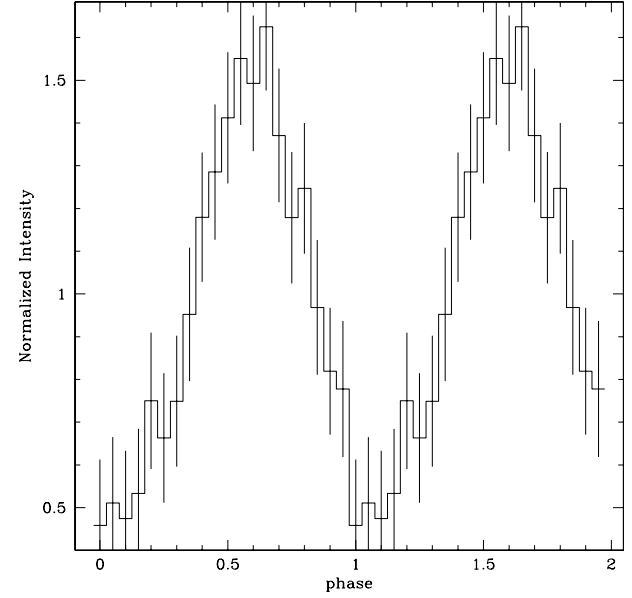
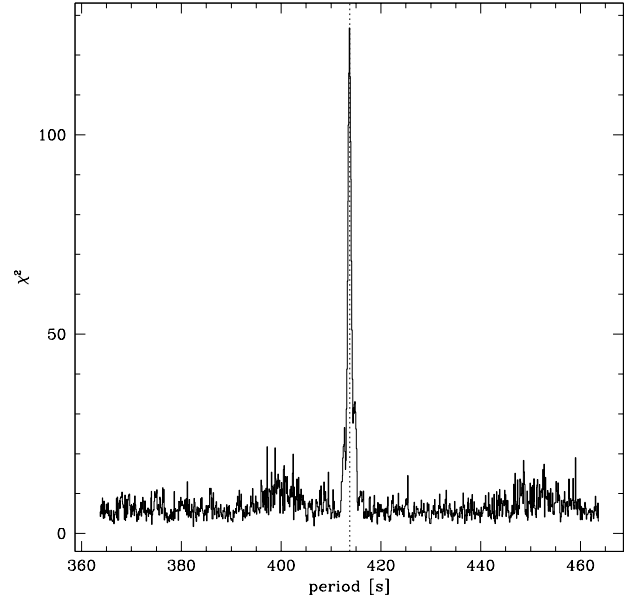


Fig. 8. *top:* IGR J17252–3616 IBIS/ISGRI epoch folding search χ^2 distribution. The best period was fitted with a Gaussian and resulted in 413.7 ± 0.3 s (see dashed-line). *bottom:* ISGRI folded light curve built with data from revolution 106 (MJD 52877.4–52880.4). IGR J17252–3616 pulse phase folded light curve in the 20–40 keV energy band was obtained with the best spin period. The zero epoch is MJD 52877.50072.

than 4 keV. An emission line at 6.4 keV and an edge at 7 keV are clearly detected. The spectra were first fitted with a simple absorbed power law and a blackbody model. In terms of reduced χ^2 , these simple models fitted the *XMM-Newton* data well. In order to distinguish between the two models, the EPIC and ISGRI spectra are used together.

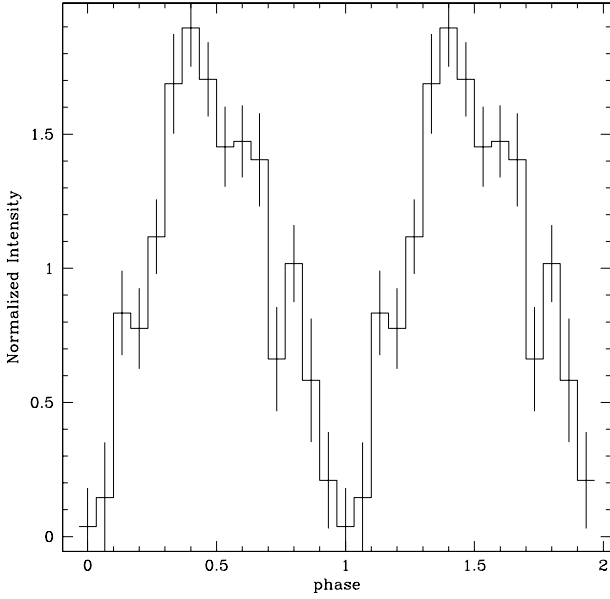


Fig. 9. IGR J17252–3616 orbital folded light curve in the 20–60 keV energy band was obtained with the best period of 9.72 d. The zero epoch is MJD 52671. The *XMM-Newton* observation correspond to phase ~ 0.7 .

The ISGRI spectrum was extracted from revolution 106 data when the source intensity was the strongest (see Fig. 5) and also from an average mosaic image of all visibility periods. The two spectra do not show any significant difference beside their normalisations. In the following spectral analysis, the revolution 106 source spectrum was used since it has the highest S/N.

When fitting EPIC and ISGRI spectra together, an inter calibration factor, C_{ISGRI} , was applied to take into account the different source flux levels during the non simultaneous observations. The simple absorbed power law and blackbody models failed to fit the data between 1–50 keV. The blackbody is too narrow and the power law requires a high-energy cutoff.

A cutoff power law (CPL) was therefore chosen as a phenomenological model to fit the data. Moreover, a more physical model based on Comptonization (CTT) (Titarchuk 1994) was also adopted as suggested by other observations (Torrejón *et al.* 2004; Bodaghee *et al.* 2005; Masetti *et al.* 2005; Walter *et al.* 2005). In Xspec, the CPL model is defined as `cst*wabs(bbody+vphabs(cutoffpl+ga))` and CTT as `cst*wabs(bbody+vphabs(compTT+ga))`. The 6.4 keV line was fitted with a Gaussian. An absorption model was used, where the iron abundance was left as a free parameter. The soft excess at low energies was modelled with a black body. The galactic absorption is also taken into account. All the spectral parameters errors were calculated at the 90% confidence level. Parameters resulting from the spectral fitting are listed in Table 2.

The CPL model gives typical values of an accreting pulsar with a flat powerlaw, $\Gamma = 0.0 \pm 0.1$, and an energy cutoff, $E_c = 8.2 \pm 0.4$ keV. The CTT model also fits the data

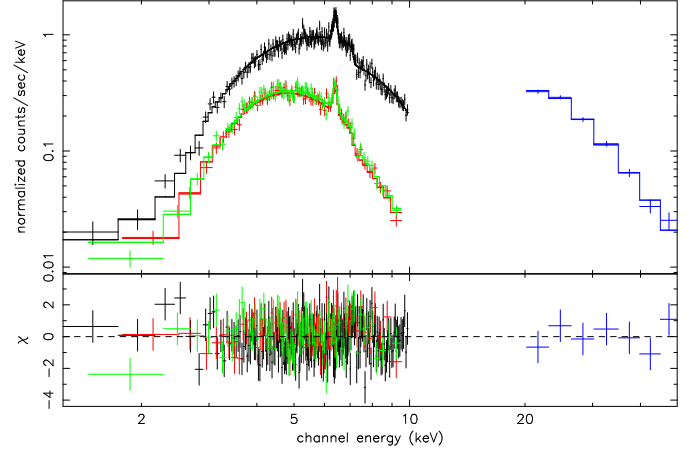


Fig. 10. Combined IGR J17252–3616 EPIC+ISGRI averaged spectrum. All three EPIC spectra are displayed in the X-ray band: pn (top) and MOS[12] (bottom). The ISGRI spectra is in the hard X-ray band. The source is detected up to 50 keV. CTT model is used.

well with characteristic values for the electron temperature of $kT_e = 5.5 \pm 0.2$ keV and an optical depth of $\tau = 7.8 \pm 0.6$. In both cases, the unabsorbed flux between 2–12 keV and 13–100 keV is 2 and 5 10^{-10} ergs $\text{cm}^{-2} \text{s}^{-1}$, respectively.

The line centroid at 6.40 ± 0.01 keV is compatible with what is expected from cold iron. The line width is consistent with zero and was fixed for the spectral fits. The equivalent width of that line is 84 eV and was calculated considering the unabsorbed continuum.

A soft excess is required below 3 keV and was represented by a blackbody absorbed by the galactic column density (without soft excess, $\chi^2/\text{d.o.f.} = 415/376$ and $420/376$ for CPL and CTT models, respectively). In this case, the 1–2 keV soft X-ray flux is 1.6 or 2.0 10^{-14} ergs $\text{cm}^{-2} \text{s}^{-1}$ (CPL or CTT). An alternative model was also used to explain the origin of the soft X-ray excess based on the idea that the absorbing matter could only partially cover the X-ray emitting source (model `pcfabs` in Xspec). A covering factor of 0.995 ± 0.002 could also explain the soft excess with a good fit of $\chi^2/\text{d.o.f.} = 406/378$ for CTT model ($411/378$ for CPL).

For phase-resolved spectroscopy with EPIC/pn, the pulse profile was cut into three phase intervals: 0.00–0.43 + 0.81–1.00 for the low intensity part, 0.43–0.49 + 0.71–0.81 for the wings of the broad pulse; 0.49–0.71 for the pulse core. The effective exposures for each phase resolved bin are 3383 s, 894 s and 1229 s, respectively. The phase-resolved spectra were extracted and the channel bins were grouped to have at least 50 counts per channel for the low intensity part and the pulse core, and 20 counts per channel for the pulse wings. All the resulting spectra were fitted inside Xspec using the CTT model again combined with the ISGRI spectrum to better constrain the spectral fit. No significant variation of the spectral shape with the phase was found, excepting the change in the normalisation (see Table 3).

Therefore, the three phase-resolved spectra were fitted with the Comptonization model and all the continuum parameters were fixed, except its normalisation, the column density, and

Table 2. Spectral analysis. The EPIC and ISGRI spectra were fitted together. Two models in Xspec were selected to fit the data. Model CPL is `constant*wabs(bbody+vphabs(cutoffpl+gaussian))` and model CTT is `constant*wabs(bbody+vphabs(compTT+gaussian))`. The galactic absorption $N_{\text{H}}^{\text{gal}}$ was fixed. The errors are calculated at the 90% confidence level.

Models	Parameters	Values	Unit
model CPL	C_{ISGRI}	2.6	
	$N_{\text{H}}^{\text{gal}}$	1.5	10^{22} cm^{-2}
	kT_{soft}	0.5	keV (fixed)
	$F_{1-2\text{keV}}$	1.6	$10^{-14} \text{ ergs cm}^{-2} \text{ s}^{-1}$
	N_{H}	$12.8^{+0.7}_{-1.3}$	10^{22} cm^{-2}
	Z_{Fe}	$1.5^{+0.2}_{-0.2}$	Z_{\odot}
	Γ	$0.02^{+0.17}_{-0.10}$	
	E_{c}	$8.2^{+0.4}_{-0.3}$	keV
	E_{line}	$6.400^{+0.001}_{-0.013}$	keV
	F_{line}	$1.9^{+0.2}_{-0.2}$	$10^{-4} \text{ ph cm}^{-2} \text{ s}^{-1}$
	unabs $F_{2-12\text{keV}}$	1.5	$10^{-10} \text{ ergs cm}^{-2} \text{ s}^{-1}$
	unabs $F_{13-100\text{keV}}$	5.1	$10^{-10} \text{ ergs cm}^{-2} \text{ s}^{-1}$
	$\chi^2/\text{d.o.f.}$	401/376	
model CTT	C_{ISGRI}	1.7	
	$N_{\text{H}}^{\text{gal}}$	1.5	10^{22} cm^{-2}
	kT_{soft}	0.5	keV (fixed)
	$F_{1-2\text{keV}}$	2.0	$10^{-14} \text{ ergs cm}^{-2} \text{ s}^{-1}$
	N_{H}	$15.3^{+1.1}_{-1.0}$	10^{22} cm^{-2}
	Z_{Fe}	$1.4^{+0.3}_{-0.3}$	Z_{\odot}
	kT_0	0.1	keV (fixed)
	kT_{e}	$5.5^{+0.2}_{-0.2}$	keV
	τ	$7.8^{+0.6}_{-0.5}$	
	E_{line}	$6.401^{+0.005}_{-0.009}$	keV
	F_{line}	$2.1^{+0.2}_{-0.3}$	$10^{-4} \text{ ph cm}^{-2} \text{ s}^{-1}$
	unabs $F_{2-12\text{keV}}$	1.7	$10^{-10} \text{ ergs cm}^{-2} \text{ s}^{-1}$
	unabs $F_{13-100\text{keV}}$	4.8	$10^{-10} \text{ ergs cm}^{-2} \text{ s}^{-1}$
	$\chi^2/\text{d.o.f.}$	401/376	

Table 3. Phase-resolved spectral analysis. We used the CTT model. All continuum and normalisation parameters were left free. A few parameters were fixed as for the average spectrum (see Table 2): $N_{\text{H}}^{\text{gal}} = 1.5 \times 10^{22} \text{ cm}^{-2}$, $kT_{\text{soft}} = 0.5 \text{ keV}$, $kT_0 = 0.1 \text{ keV}$. Only pn data were used for the phase-resolved spectral analysis.

Parameters	low intensity	pulse wings	pulse core	Unit
C_{ISGRI}	2.6	1.4	0.9	
$F_{1-2\text{keV}}$	1.4	4.2	2.8	$10^{-14} \text{ ergs cm}^{-2} \text{ s}^{-1}$
N_{H}	$15.2^{+2.0}_{-2.2}$	$13.7^{+2.9}_{-2.6}$	$15.1^{+1.8}_{-1.8}$	10^{22} cm^{-2}
Z_{Fe}	$1.2^{+0.6}_{-0.5}$	$2.0^{+1.2}_{-0.8}$	$1.6^{+0.5}_{-0.4}$	Z_{\odot}
kT_{e}	$5.5^{+0.2}_{-0.2}$	$5.4^{+0.2}_{-0.2}$	$5.5^{+0.2}_{-0.2}$	keV
τ	$8.0^{+1.0}_{-0.8}$	$8.7^{+1.5}_{-1.2}$	$7.8^{+0.8}_{-0.7}$	
E_{line}	$6.40^{+0.01}_{-0.02}$	$6.42^{+0.04}_{-0.03}$	$6.40^{+0.04}_{-0.05}$	keV
F_{line}	$2.2^{+0.3}_{-0.3}$	$1.6^{+0.6}_{-0.6}$	$1.4^{+0.7}_{-0.6}$	$10^{-4} \text{ ph cm}^{-2} \text{ s}^{-1}$
unabs $F_{2-12\text{keV}}$	1.2	2.0	3.4	$10^{-10} \text{ ergs cm}^{-2} \text{ s}^{-1}$
$\chi^2/\text{d.o.f.}$	145/160	208/217	180/197	

the soft excess and the line normalisations. The results are summarized in Table 4. No significant variation of the line flux nor of the absorbing column density was observed. The unabsorbed 2–10 keV flux changes according to the pulse phase. The variations of the 1–2 keV flux are not significant once the errors are considered.

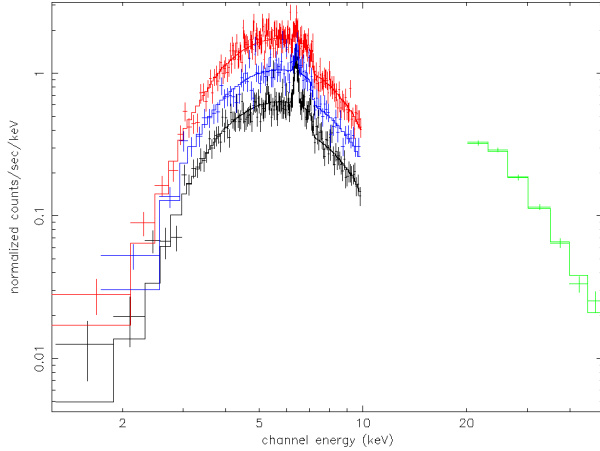
5. Discussion

5.1. X-ray counterpart

When IGR J17252–3616 was discovered in the γ -rays, it was first labelled as a new source since no other known sources lay within the ISGRI error circle of $2'$. The nearest source was EXO 1722–363 at a distance of $12'$. The EXOSAT source was considered to be too far to be the X-ray counterpart of IGR J17252–3616. With the improved ISGRI and EPIC po-

Table 4. Phase-resolved spectroscopy with all the spectral modeling parameters of model CTT except normalisations equal to the values of the average spectrum (see Table 2). Only pn data were used for the phase-resolved spectral analysis.

phase	N_{H} 10^{22} cm^{-2}	F_{line} $10^{-4} \text{ ph cm}^{-2} \text{ s}^{-1}$	$F_{1-2 \text{ keV}}$ $10^{-14} \text{ ergs cm}^{-2} \text{ s}^{-1}$	unabsorbed $F_{2-10 \text{ keV}}$ $10^{-10} \text{ ergs cm}^{-2} \text{ s}^{-1}$	$\chi^2/\text{d.o.f}$
low intensity	$15.3^{+0.7}_{-0.7}$	$2.1^{+0.4}_{-0.3}$	$1.5^{+1.5}_{-1.2}$	0.9	147/164
pulse wings	$15.8^{+1.3}_{-0.7}$	$1.5^{+0.7}_{-0.6}$	$6.8^{+0.4}_{-4.9}$	1.4	214/221
pulse core	$15.5^{+0.5}_{-0.5}$	$1.6^{+0.5}_{-0.7}$	$2.8^{+2.2}_{-2.2}$	2.4	181/201

**Fig. 11.** EPIC/pn phase-resolved spectra. Only the pn spectra of the three phase intervals are displayed in the X-ray band: low intensity (bottom), pulse wings (middle) and pulse core (top). The ISGRI spectrum in the hard X-ray band is not phase resolved.

sition, the source still lies $12'$ away from the given EXOSAT position with an accuracy of $9'$ (Warwick *et al.* 1988).

Tawara *et al.* (1989) also gave a new position within a box of $2^\circ \times 4^\circ$ that is $20'$ away from the EPIC position. They discovered a pulsation of 413.9 s. The pulse profile shows a single peak that is independent of the energy and a high pulse fraction of 80%. The spectrum is heavily absorbed at low energy and shows a very hard shape plus an emission line at 6.2 ± 0.5 keV. Even if the position given by all these studies is quite far from the accurate IGR J17252–3616 position, the informations given by Tawara *et al.* (1989) strongly confirm that the same source is seen since the same features are seen in this study.

From archival data of RXTE/PCA taken between 1999 and 2003, Markwardt & Swank (2003) reported an orbital period of 9.737 ± 0.004 days, consistent with the lower limit given by Takeuchi *et al.* (1990). This result with RXTE was confirmed by Corbet *et al.* (2005). Their best orbital period is 9.741 ± 0.004 d. They also find a pulse period of 413.88553 ± 0.00001 s, equivalent to the previous studies and with the measurement presented here.

5.2. Temporal modulations

In this paper, periodic or episodic time variations were searched for on time scales of seconds to days. First, the two years long ISGRI 20–60 keV light curve indicates that the source is persistent. However, variations in the γ -ray count rates larger than

50 were observed for this system. Four flares were detected on a time scale of hours.

An orbital period of 9.72 ± 0.09 days was derived that is consistent with the one derived by Corbet *et al.* (2005). The eclipse duration is a bit lower in the ISGRI data than in the RXTE data (~ 1.3 days and ~ 1.7 days respectively). Both orbital profile at 2–10 keV and 20–60 keV are consistent. The progressive decrease of the intensity before entering the eclipse between phase 0.7 and 0.97 can be explained by the changing hydrogenic column density that increases from $\sim 10^{23} \text{ cm}^{-2}$ to $\sim 10^{24} \text{ cm}^{-2}$. This larger amount of matter along the line of sight implies that a larger part of the flux is scattered.

Similar pulsations were found in EPIC/pn and ISGRI data: 414.8 ± 0.5 s and 413.7 ± 0.3 s, respectively. The EPIC and ISGRI pulsations are consistent with the one detected by Tawara *et al.* (1989) and Corbet *et al.* (2005). Therefore, the spin period did not change significantly in the last 17 years. Takeuchi *et al.* (1990) also searched for pulse period changes and did not find any significant spin variation in Ginga data. The neutron star seems to not accrete kinetic momentum, which suggests accretion from a stellar wind.

With such spin pulsation and orbital period, the source is situated in the underfilled Roche-Lobe supergiant region in the P_{spin} vs P_{orb} Corbet diagram (Corbet 1986). Together with the fact that the source is persistent and shows non-periodic flares with different intensities, this strongly suggests that IGR J17252–3616 is a high mass system fed by stellar wind with the primary star being a supergiant.

5.3. Spectra

The EPIC and ISGRI spectra that could be well fitted with a flat power law ($\Gamma \sim 0$) and an energy cutoff at $E_c = 8.2$ keV are typical of X-ray pulsars (White *et al.* 1995). Three spectral features can give more clues about the physics of this object: the apparent soft excess, the huge hydrogen column density and the cold Fe $K\alpha$ line.

A soft excess is detected below 2 keV. Such soft X-ray excess has been observed in other HMXB (Hickox *et al.* 2004). It could originate in X-ray scattering or partial ionization in the stellar wind (White *et al.* 1995). The spectrum at soft X-rays could also be explained by a partial covering of the X-ray source by the absorbing matter. In the latter case, pulsations at soft X-rays would be expected. The 0.4–2 keV light curve was extracted and folded using the same ephemeris and period used to fold the 0.4–10 keV light curve. Then, it was compared to a constant model with $\chi^2/\text{d.o.f.} \sim 57/50$ and the 0.4–10 keV pulse profile with $\chi^2/\text{d.o.f.} \sim 54/50$. Both models are compati-

ble with the 0.4–2 keV folded light curve. However, the number of events gathered below 2 keV is too poor to decide if the soft excess is pulsating or not.

The absorbing column density was estimated at $13\text{--}15 \times 10^{22}$ atoms cm^{-2} (model CPL-CTT) that is ten times larger than expected on the line of sight $N_{\text{H}} = 1.5 \times 10^{22}$ atoms cm^{-2} . This high absorption could be explained by the stellar wind expelled by the primary star that surrounds the neutron star. During the *XMM-Newton* observation, the column density did not vary with the pulse. The fact that the amount of matter did not change noticeably during the 10 ks *XMM-Newton* observation could indicate that the surrounding matter is stable on this time scale. However, other values of the column density were reported at different epochs by Tawara *et al.* (1989), Takeuchi *et al.* (1990) and Corbet *et al.* (2005). The column density has been observed to increase up to 10^{24} atoms cm^{-2} in the past. This could be related to the neutron star moving along the orbit (Tawara *et al.* 1989; Corbet *et al.* 2005). Therefore, the matter does not homogeneously surround the binary system. Instabilities in the stellar wind of the companion star could also be responsible for this evolving absorption. However, in Corbet *et al.* (2005), the column density seems to be linked to the orbital phase where the highest values correspond to the exit of the eclipse and the lowest ones when the source is in front of the companion star. The absorption is therefore intrinsic to the binary system.

The 6.4 keV Fe $K\alpha$ line is detected. The Fe $K\alpha$ line flux does not vary with the pulse phase (see Table 4). Therefore, either the matter responsible for the fluorescence is homogeneously distributed around the source or the thickness of the shell emitting the fluorescence is larger than 1.2×10^8 km around the accreting system. The Fe $K\alpha$ line energy is $6.401^{+0.005}_{-0.009}$ keV (CTT model) and corresponds to iron that is at most 12 times ionized (House 1969). An upper limit of the ionization parameter can be estimated as $\log(L/nR^2) < 1$, where L is the luminosity, n the gas density, and R is the distance from the ionizing continuum source to the inner shell surface (Kallman *et al.* 2004). Since $nR \sim N_{\text{H}}$, the distance of the fluorescence source from the X-ray source is larger than 10^7 km. The values derived for the hydrogen column density, the equivalent width, and the estimated over abundance of iron are compatible with a spherical distribution of matter around the source (Matt 2002).

Considering a typical luminosity of an active accretion-powered pulsars of 1.2×10^{36} ergs s^{-1} (Bildsten *et al.* 1997), the distance of IGR J17252–3616 can be estimated as 7 kpc, close to the galactic centre.

6. Conclusions

IGR J17252–3616 is the hard X-ray counterpart of EXO 1722–363, and the most accurate source position to date has been provided here. IGR J17252–3616 has been monitored by *INTEGRAL* during two years for a total exposure of 6.5 Ms and *XMM-Newton* performed a follow-up observation of 3 hours. The source is persistent with an average 20–60 keV flux of 6.4 mCrab. Four flares lasting less than one day were detected by *INTEGRAL*. The source’s count rate varies by a factor larger than 50 on such timescales. A

pulsation has been detected in both EPIC and IBIS/ISGRI data of 414.8 ± 0.5 s and 413.7 ± 0.3 s, respectively. There is no evidence of spin period variation. An orbital period of 9.72 ± 0.09 d is also found in IBIS/ISGRI data. The spectral shape is typical for an accreting pulsar except that a huge intrinsic absorption and a cold iron fluorescence line are detected. The absorbing column density and cold iron line do not vary with the pulse period. The absorbing fluorescent material is distributed around the neutron star in a shell comparable in size with the orbital radius. With the accurate X-ray position, we provide a likely infra-red counterpart within the X-ray error box: 2MASS J17251139–3616575. The observed features of the source suggest that it is a wind-fed accreting pulsar. This object is a new member of the growing family of heavily-obscured HMXB systems that have been recently discovered with *INTEGRAL*. The source is located ~ 7 kpc away, near the Galactic Centre.

Acknowledgements. Based on observations obtained with the ESA science missions *INTEGRAL* and *XMM-Newton*. The *INTEGRAL* and *XMM-Newton* instruments and data centres were directly funded by ESA member states and the USA (NASA). JAZH thanks J.Rodriguez for his useful comments and N.Produit for his help with *ii_light*.

References

- Bildsten, L., Chakrabarty, D., Chiu, J., et al. 1997, *ApJS*, 113, 367
- Bird, A. J., Barlow, E. J., Bassani, L., et al. 2004, *ApJ*, 607, L33
- Bodaghee, A., Walter, R., Zurita Heras, J. A., et al. 2005, accepted for publication in *A&A*
- Corbet, R. H. D. 1986, *MNRAS*, 220, 1047
- Corbet, R. H. D., Markwardt, C. B., & Swank, J. H. 2005, *ApJ*, in press
- Courvoisier, T. J.-L., Walter, R., Beckmann, V., et al. 2003, *A&A*, 411, L53
- Cutri, R. M., Skrutskie, M. F., van Dyk, S., et al. 2003, *VizieR Online Data Catalog*, 2246, 0
- Gros, A., Goldwurm, A., Cadolle-Bel, M., et al. 2003, *A&A*, 411, L179
- Hickox, R. C., Narayan, R., & Kallman, T. R. 2004, *ApJ*, 614, 881
- Hill, A. B., Walter, R., Knigge, C., et al. 2005, *A&A*, 439, 255
- Horne, J. H. & Baliunas, S. L. 1986, *ApJ*, 302, 757
- House, L. L. 1969, *ApJS*, 18, 21
- Jansen, F., Lumb, D., Altieri, B., et al. 2001, *A&A*, 365, L1
- Kallman, T. R., Palmeri, P., Bautista, M. A., Mendoza, C., & Krolik, J. H. 2004, *ApJS*, 155, 675
- Labanti, C., Di Cocco, G., Ferro, G., et al. 2003, *A&A*, 411, L149
- Lebrun, F., Leray, J. P., Lavocat, P., et al. 2003, *A&A*, 411, L141
- Lund, N., Budtz-Jørgensen, C., Westergaard, N. J., et al. 2003, *A&A*, 411, L231
- Markwardt, C. B. & Swank, J. H. 2003, *The Astronomer’s Telegram*, 179, 1
- Mas-Hesse, J. M., Giménez, A., Culhane, J. L., et al. 2003, *A&A*, 411, L261

- Masetti, N., Orlandini, M., Dal Fiume, D., et al. 2005, *astro-ph/0508451*, accepted for publication in *Å*
- Matt, G. 2002, *MNRAS*, 337, 147
- Patel, S. K., Kouveliotou, C., Tennant, A., et al. 2004, *ApJ*, 602, L45
- Press, W. H. & Rybicki, G. B. 1989, *ApJ*, 338, 277
- Rodriguez, J., Tomsick, J. A., Foschini, L., et al. 2003, *A&A*, 407, L41
- Strüder, L., Briel, U., Dennerl, K., et al. 2001, *A&A*, 365, L18
- Takeuchi, Y., Koyama, K., & Warwick, R. S. 1990, *PASJ*, 42, 287
- Tauris, T. M. & van den Heuvel, E. P. J. 2005, *Formation and Evolution of Compact Stellar X-ray Sources (Compact Stellar X-Ray Sources*, eds. W.H.G. Lewin and M. van der Klis, Cambridge University Press), in press
- Tawara, Y., Yamauchi, S., Awaki, H., et al. 1989, *PASJ*, 41, 473
- Titarchuk, L. 1994, *ApJ*, 434, 570
- Torrejón, J. M., Kreykenbohm, I., Orr, A., Titarchuk, L., & Negueruela, I. 2004, *A&A*, 423, 301
- Turner, M. J. L., Abbey, A., Arnaud, M., et al. 2001, *A&A*, 365, L27
- Ubertini, P., Lebrun, F., Di Cocco, G., et al. 2003, *A&A*, 411, L131
- Vedrenne, G., Roques, J.-P., Schönfelder, V., et al. 2003, *A&A*, 411, L63
- Walter, R., Bodaghee, A., Barlow, E. J., et al. 2004, *The Astronomer's Telegram*, 229, 1
- Walter, R., Rodriguez, J., Foschini, L., et al. 2003, *A&A*, 411, L427
- Walter, R., Zurita Heras, J. A., Bassani, L., et al. 2005, submitted to *A&A*
- Warwick, R. S., Norton, A. J., Turner, M. J. L., Watson, M. G., & Willingale, R. 1988, *MNRAS*, 232, 551
- White, N. E., Nagase, F., & Parmar, A. N. 1995, *X-ray binaries (Cambridge Astrophysics Series, Cambridge, MA: Cambridge University Press, —c1995, edited by Lewin, Walter H.G.; Van Paradijs, Jan; Van den Heuvel, Edward P.J.)*, 1–57
- Winkler, C., Courvoisier, T. J.-L., Di Cocco, G., et al. 2003, *A&A*, 411, L1